MIMO Channel Hardening for Ray-based Models

Matthieu Roy[†], Stéphane Paquelet[†], Luc Le Magoarou[†], Matthieu Crussière[‡]
[†]b<>com Rennes, France, firstname.lastname@b-com.com
[‡]Univ Rennes, INSA Rennes, IETR - UMR 6164 F-35000 Rennes, France

***Abstract*—In a multiple-input-multiple-output (MIMO) communication system, the multipath fading tends to vanish with increasing number of radio links. This well-known *channel hardening* phenomenon plays a central role in the design of massive MIMO systems. It is quantified by the coefficient of variation of the channel gain. The aim of this paper is to study channel hardening using a physical channel model in which the influences of propagation rays and antenna array topologies are highlighted. Our analyses and closed form results extend the *hardening properties* beyond the classical Rayleigh fading models and offer further insights on the relationship with channel characteristics.**

***Index Terms*—channel hardening, physical model, MIMO**

I. Introduction

Over the last decades, multi-antenna techniques have been identified as key technologies to improve the throughput and reliability of future communication systems. They offer a potential massive improvement of spectral efficiency over classical SISO (single-input-single-output) systems proportionally to the number of involved antennas. This promising gain has been quantified in terms of capacity in the seminal work of Telatar [1] and has recently been even more emphasized with the newly introduced massive MIMO paradigm [2].

Moving from SISO to MIMO, the reliability of communication systems improves tremendously. On the one hand in SISO, the signal is emitted from one single antenna and captured at the receive antenna as a sum of constructive or destructive echoes. This results in fading effects leading to a potentially very unstable signal to noise ratio (SNR) depending on the richness of the scattering environment. On the other hand in a MIMO system, with appropriate precoding, small-scale multipath fading is averaged over the multiple transmit and receive antennas. This yields a strong reduction of the received power fluctuations, hence the channel gain becomes locally deterministic essentially driven by its large-scale properties (namely path-loss and shadowing). This effect referred to as *channel hardening* [3] has recently been given a formal definition based on the channel power fluctuations [4]. Indeed, studies on the stability of the SNR are essential to the practical design of MIMO systems, in particular on scheduling, rate feedback, channel coding and modulation dimensioning [2], [3], [5]. From the definition in [4], we propose in this paper a comprehensive study on channel hardening through a statistical analysis of received power variations derived from the propagation characteristics of a generic ray-based spatial channel model.

Related work. Channel hardening, measured as the channel gain variance, has recently been studied from several points of view. The authors in [6] and [7] used data from measurement campaigns and extracted the variance of the received power. A rigorous definition of channel hardening was then given in the seminal work [4] based on the asymptotic behavior of the channel gain for large antenna arrays. This definition was applied to pinhole channels, i.i.d. correlated and uncorrelated Rayleigh fading models [8].

Contributions. Complementary to this pioneer work, we propose a non-asymptotic analysis of channel hardening, as well as new derivations of the coefficient of variation of the channel not limited to classically assumed Rayleigh fading models. Indeed, channel hardening is analyzed herein using a physically motivated ray-based channel model widely used in wave propagation. Our approach is consistent with previous studies [4], [6], but gives deeper insights on channel hardening. Namely through the geometric description of the channel we include in our model both rich and sparse scattering propagation conditions, thus extending channel hardening evaluation beyond the classical Rayleigh fading approach. Furthermore our expression allows for exhibiting the channel hardening dependency on transmit and receive antenna array characteristics: array types, number of antennas, inter-antenna spacing.

This paper is organized as follows. Both MIMO channel gain and ray-based model are introduced in Section II. Channel hardening is defined and quantified in Section III. The expression of channel hardening for the ray-based model is derived in Section IV and analyzed in Section V where influences of antenna array topologies parameters and propagation conditions are highlighted. The correlated Rayleigh channel and ray-based model approaches and results are then compared and we finally draw a conclusion in Section VI.

Notations. Upper case and lower case bold symbols are used for matrices and vectors. z^* denotes the conjugate of z. $\vec{u}$ stands for a three-dimensional (3D) vector. $\langle .,. \rangle$ and $\vec{a} \cdot \vec{u}$ denote the inner product between two vectors of $\mathbb{C}^N$ and 3D vectors, respectively. $[\mathbf{H}]_{p,q}$ is the element of matrix $\mathbf{H}$ at row p and column q. $\|\mathbf{H}\|_F$, $\|\mathbf{h}\|$ and $\|\mathbf{h}\|_p$ stand for the Frobenius norm, the euclidean norm and the p-norm, respectively. $\mathbf{H}^H$ and $\mathbf{H}^T$ denotes the conjugate transpose and the transpose matrices. $\bar{\mathbf{H}}$ denote the normalized matrix $\mathbf{H}/||\mathbf{H}||_F$. $\mathbb{E}\{.\}$ and $\mathbb{V}\mathrm{ar}\{.\}$ denote the expectation and variance.

II. Channel Model

We consider a narrowband MU-MIMO system (interpretable as an OFDM subcarrier) with N_t antennas at the transmitter (base station) and N_r antennas for each user. $\mathbf{H}_k \in \mathbb{C}^{N_r \times N_t}$ is the MIMO channel matrix of user k,

whose entries $[\mathbf{H}_k]_{i,j}$ are the complex gains of the SISO links between transmit antenna j and receive antenna i. The capacity of the MIMO channel of user k can be expressed as

$$C_k = \log_2 \left(\left| \mathbf{I}_{N_t} + \frac{\rho_k \bar{\mathbf{Q}}_k \bar{\mathbf{H}}_k^H \bar{\mathbf{H}}_k}{\mathbf{I}_{N_t} + \sum_{i \neq k} \rho_i \bar{\mathbf{Q}}_i \bar{\mathbf{H}}_k^H \bar{\mathbf{H}}_k} \right| \right) \quad bps/Hz,$$

where $\rho_k = \frac{P_k}{N_0} ||\mathbf{H}_k||_F^2$ with $\bar{\mathbf{Q}}_k \in \mathbb{C}^{N_t \times N_t}$, P_k and N_0 the input correlation matrix (precoding), emitted power and noise power of user k. C is a monotonic function of the optimal received SNR ρ_k [9], hence $\|\mathbf{H}_k\|_F^2$ directly influences the capacity of the MIMO channel, especially in the well documented case where each user has one antenna. It is then of high interest studying the spatial channel gain variations to predict the stability of the capacity. In this paper, the variations of the channel gain of a user k are studied in a very general context. As a consequence, particularizing the study for a specific user k in the system is not required and for simplicity reasons we denote $\|\mathbf{H}\|_F^2$ instead of $\|\mathbf{H}_k\|_F^2$ the channel gain. The results are equally valid for any user.

In the sequel, we will consider that the channel matrix $\mathbf{H}$ is obtained from the following generic multi-path 3D ray-based model considering planar wavefronts [10], [11], [8, p. 485]

$$\mathbf{H} = \sqrt{N_t N_r} \sum_{p=1}^{P} c_p \mathbf{e_r}(\vec{u}_{rx,p}) \mathbf{e_t}(\vec{u}_{tx,p})^H. \tag{1}$$

Such channel consists of a sum of P physical paths where c_p is the complex gain of path p and $\vec{u}_{tx,p}$ (resp. $\vec{u}_{rx,p}$) its direction of departure - DoD - (resp. of arrival - DoA -). In (1) $\mathbf{e_t}$ and $\mathbf{e_r}$ are the so-called *steering vectors* associated to the transmit and receive arrays. They contain the path differences of the plane wave from one antenna to another and are defined as [11]

$$\mathbf{e_t}(\vec{u}_{tx,p}) = \frac{1}{\sqrt{N_t}} \left[\mathrm{e}^{2j\pi \frac{\vec{a}_{tx,1} \cdot \vec{u}_{tx,p}}{\lambda}}, \cdots, \mathrm{e}^{2j\pi \frac{\vec{a}_{tx,N_t} \cdot \vec{u}_{tx,p}}{\lambda}} \right]^T, \tag{2}$$

and similarly for $\mathbf{e_r}(\vec{u}_{rx,p})$. The steering vectors depend not only on the DoD/DoA of the corresponding rays, but also on the topology of the antenna arrays. The latter are defined by the sets of vectors $\mathcal{A}_{tx} = \{\vec{a}_{tx,j}\}$ and $\mathcal{A}_{rx} = \{\vec{a}_{rx,j}\}$ representing the positions of the antenna elements in each array given an arbitrary reference.

Such channel model has already been widely used (especially in its 2D version) [10], [11], verified through measurements [12] for millimeter waves and studied in the context of channel estimation [13]. In contrast to Rayleigh channels, it explicitly takes into account the propagation conditions and the topology of the antenna arrays.

In the perspective of the following sections, let $\mathbf{c} = [|c_1|, \cdots, |c_P|]^T$ denote the vector consisting of the amplitudes of the rays. $\|\mathbf{c}\|^2$ is the aggregated power from all rays, corresponding to large-scale fading due to path-loss and shadowing.

III. Channel Hardening

A. Definition

Due to the multipath behavior of propagation channels, classical SISO systems suffer from a strong fast fading phenomenon at the scale of the wavelength resulting in strong capacity fluctuations. MIMO systems average the fading phenomenon over the antennas so that the channel gain varies much more slowly. This effect is called *channel hardening*. In this paper, the relative variation of the channel gain $\|\mathbf{H}\|_F^2$, called coefficient of variation (CV) is evaluated to quantify the channel hardening effect as previously introduced in [4], [8]:

$$CV^2 = \frac{\mathbb{V}\mathrm{ar}\left\{\|\mathbf{H}\|_F^2\right\}}{\mathbb{E}\left\{\|\mathbf{H}\|_F^2\right\}^2} = \frac{\mathbb{E}\left\{\|\mathbf{H}\|_F^4\right\} - \mathbb{E}\left\{\|\mathbf{H}\|_F^2\right\}^2}{\mathbb{E}\left\{\|\mathbf{H}\|_F^2\right\}^2} \tag{3}$$

In (3) the statistical means are obtained upon the model which govern the entries of $\|\mathbf{H}\|^2$ given random positions of the transmitter and the receiver, the lower the better. This measure was previously applied to a $N_t \times 1$ correlated Rayleigh channel model $\mathbf{h} \sim \mathcal{CN}(\mathbf{0}, \mathbf{R})$ [4], [8, p. 231]. In that particular case, (3) becomes

$$CV^2 = \frac{\mathbb{E}\left\{|\mathbf{h}^H \mathbf{h}|^2\right\} - \mathrm{Tr}(\mathbf{R})^2}{\mathrm{Tr}(\mathbf{R})^2} = \frac{\mathrm{Tr}(\mathbf{R}^2)}{\mathrm{Tr}(\mathbf{R})^2}, \tag{4}$$

where the rightmost equality comes from the properties of Gaussian vectors [8, Lemma B.14]. This result only depends on the covariance matrix $\mathbf{R}$, from which the influences of antenna array topology and propagation conditions are not explicitly identified. Moreover, small-scale and large-scale phenomena are not easily separated either. In this paper, (3) is studied using a physical channel model that leads to much more interpretable results.

B. Interpretation and limit of correlated Rayleigh models

The previously given expression of channel hardening for correlated Rayleigh fading channels is bounded by

$$\frac{1}{N_r N_t} \leq CV^2_{Rayleigh} = \frac{\mathrm{Tr}(\mathbf{R}^2)}{\mathrm{Tr}(\mathbf{R})^2} \leq 1$$

where the rightmost inequality is attained for $\mathrm{rank}(\mathbf{R}) = 1$ and the leftmost one for $\mathbf{R} = \mathbf{Id}$. With such model, the measure of channel hardening is completely defined by the distribution of the correlation matrix eigenvalues.

The unit rank case can for example be obtained when the antenna spacing is reduced. It is indeed well-known that antenna spacing below the half-wavelength leads to a reduced rank correlation matrix thus decreases the channel hardening effect. In contrast, the full rank situation corresponds to the limit obtained for uncorrelated entries of matrix $\mathbf{H}$, that is when the number of rays becomes sufficiently large.

However millimeter waves propagation yields only a small amount of clusters reducing the small-scale scattering effect. For instance NYUSIM channel model realizations [14] usually exhibits from one to six main time clusters and from one to five spatial lobes. The correlated Rayleigh models assume an

asymptotically high number of rays. Hence it is not suitable for MIMO channel hardening studies in a millimeter wave context.

Studying channel hardening with a physical channel model is necessary to provide more insights by separating antenna array topologies and propagation characteristics.

C. Assumptions on the channel model

The multipath channel model described in Section II relies on several parameters governed by some statistical laws. Our aim is to provide an analytical analysis of CV while relying on the weakest possible set of assumptions on the channel model. Hence, we will consider that:

- For each ray, gain, DoD and DoA are independent.
- The phases $\arg(c_p) \sim \mathcal{U}[0, 2\pi]$ are i.i.d.
- Both DoD $\vec{u}_{tx,p}$ and DoA $\vec{u}_{rx,p}$ are i.i.d. with distributions $\mathcal{D}_{tx}$ and $\mathcal{D}_{rx}$.

The first hypothesis is widely used and simply says that no formal relation exists between the gain and the DoD/DoA of each ray. The second one reasonably indicates that each propagated path experiences independent phase rotation without any predominant angle. The last one assumes that all the rays come from independent directions, with the same distribution (distributions $\mathcal{D}_{tx}$ at the emitter, $\mathcal{D}_{rx}$ at the receiver).

It has indeed been observed through several measurement campaigns that rays can be grouped into clusters [15], [16]. Considering the limited angular resolution of finite-size antenna arrays, it is possible to approximate all rays of the same cluster as a unique ray without harming a lot the channel description accuracy [13]. It then makes sense to assume that this last hypothesis is valid for the main DoDs and DoAs of the clusters.

D. Simulations

A preliminary assessment of the coefficient of variation is computed through Monte-Carlo simulations of (3) using uniform linear arrays (ULA) with inter-antenna spacing of $\frac{\lambda}{2}$ at both the transmitter and receiver and taking a growing number of antennas. A total of $P \in \{2, 4, 6, 8\}$ paths were randomly generated with Complex Gaussian gains $c_p \sim \mathcal{CN}(0, 1)$, uniform DoDs $\vec{u}_{tx,p} \sim \mathcal{U}_{\mathcal{S}_2}$ and DoAs $\vec{u}_{rx,p} \sim \mathcal{U}_{\mathcal{S}_2}$.

Simulation results of CV are reported in Fig. 1 as a function of the number of antennas. It is observed that all curves have a variable component and a constant component. Those two components have opposite behaviors. The variable one decreases faster in stronger scattering cases and vanishes for high number of antennas. The constant one have the opposite behavior and is higher for low scattering scenarios. One should keep in mind that those simulations embraces a wide variety of situations with various path-loss, shadowing and fading. We will explicitly state later on that this constant component is due to large-scale characteristics (path-loss and shadowing). The goal of the next sections is to provide further interpretation of such phenomenon by means of analytical derivations.

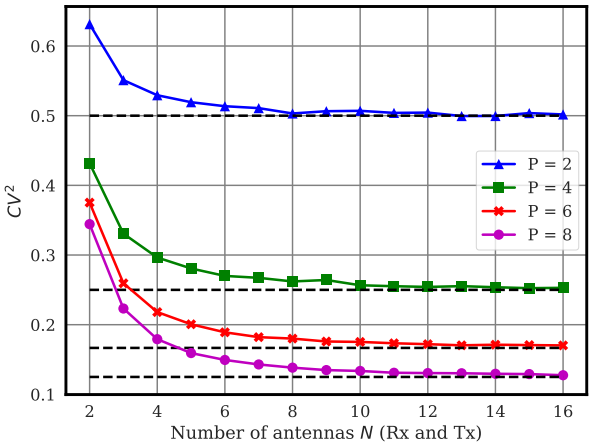


Fig. 1. Simulated CV^2 for growing number of rays. Asymptotes are the black dashed lines.

IV. Derivation of CV^2

In this section, CV^2 is analytically analyzed from (3).

Expectation of the channel gain. From (1) and (2) the channel gain $\|\mathbf{H}\|_F^2 = \mathrm{Tr}(\mathbf{H}^H\mathbf{H})$ can be written as

$$\|\mathbf{H}\|_F^2 = N_t N_r \sum_{p,p'} c_p^* c_{p'} \gamma_{p,p'},$$

where the term $\gamma_{p,p'}$ is given by

$$\gamma_{p,p'} = \langle \mathbf{e_r}(\vec{u}_{rx,p}), \mathbf{e_r}(\vec{u}_{rx,p'})\rangle \langle \mathbf{e_t}(\vec{u}_{tx,p}), \mathbf{e_t}(\vec{u}_{tx,p'})\rangle^*.$$

Using the hypothesis $\arg(c_p) \sim \mathcal{U}[0, 2\pi]$ i.i.d. introduced in the channel model and $\gamma_{p,p} = 1$, the expectation of the channel gain can further be expressed as

$$\mathbb{E}\left\{\|\mathbf{H}\|_F^2\right\} = N_t N_r \mathbb{E}\left\{\|\mathbf{c}\|^2\right\}. \tag{5}$$

Thus the average channel gain increases linearly with N_r and N_t, which is consistent with the expected beamforming gain N_t and the fact that the received power linearly depends on N_r.

Coefficient of variation. The coefficient of variation CV is derived using the previous hypotheses and (5). We introduce:

$$\begin{cases} \mathcal{E}^2(\mathcal{A}_{tx}, \mathcal{D}_{tx}) = \mathbb{E}\left\{|\langle \mathbf{e_t}(\vec{u}_{tx,p}), \mathbf{e_t}^*(\vec{u}_{tx,p'})\rangle|^2\right\} \\ \mathcal{E}^2(\mathcal{A}_{rx}, \mathcal{D}_{rx}) = \mathbb{E}\left\{|\langle \mathbf{e_r}(\vec{u}_{rx,p}), \mathbf{e_r}(\vec{u}_{rx,p'})\rangle|^2\right\} \end{cases} \tag{6}$$

which depend on the topologies of the antenna arrays defined by the sets of vectors previously defined $\mathcal{A}_{tx}$, $\mathcal{A}_{rx}$ and on the distributions of the DoDs and DoAs $\mathcal{D}_{tx}$, $\mathcal{D}_{rx}$. These quantities are the second moments of the inner products of the transmit/receive steering vectors associated to two distinct rays. They represent the correlation between two rays as observed by the system. They can also be interpreted as the average inability of the antenna arrays to discriminate two rays given a specific topology and ray distribution. From such

definitions, and based on the derivations given in Appendix A, CV^2 can be expressed as a sum of two terms,

$$CV^2 = \mathcal{E}^2(\mathcal{A}_{tx},\mathcal{D}_{tx})\mathcal{E}^2(\mathcal{A}_{rx},\mathcal{D}_{rx})\frac{\mathbb{E}\left\{\|\mathbf{c}\|^4 - \|\mathbf{c}\|_4^4\right\}}{\mathbb{E}\left\{\|\mathbf{c}\|^2\right\}^2} + \frac{\mathbb{V}\mathrm{ar}\left\{\|\mathbf{c}\|^2\right\}}{\mathbb{E}\left\{\|\mathbf{c}\|^2\right\}^2}. \quad (7)$$

Note that this result only relies on the assumptions introduced in section II. The second term can be identified as the contribution of the spatial large-scale phenomena since it simply consists in the coefficient of variation of the previously defined large-scale fading parameter $\|\mathbf{c}\|^2$ of the channel. To allow local channel behavior interpretation, conditioning the statistical model by $\|\mathbf{c}\|^2$ is required. It results in the cancellation of the large-scale variations contribution of CV^2 which reduces to the first term identified as what is called hereafter *small-scale fading*.

V. Interpretations

A. Large-scale fading

The contribution of large-scale fading in CV^2 is basically the coefficient of variation of the total aggregated power $\|\mathbf{c}\|^2$ of the rays. To better emphasize its behavior, let us consider a simple example with independent $|c_p|^2$ of mean μ and variance σ^2. The resulting large scale fading term is then

$$\frac{\mathbb{V}\mathrm{ar}\left\{\|\mathbf{c}\|^2\right\}}{\mathbb{E}\left\{\|\mathbf{c}\|^2\right\}^2} = \frac{1}{P}\left(\frac{\sigma}{\mu}\right)^2.$$

It clearly appears that more rays lead to reduced large-scale variations. This stems from the fact that any shadowing phenomenon is well averaged over P independent rays, hence becoming almost deterministic in rich scattering environments. This result explains the floor levels obtained for various P in our previous simulations in Section III-D and is consistent with the literature on correlated Rayleigh fading channels where high rank correlation matrices provide a stronger channel hardening effect than low rank ones [8] as previously discussed in III-B.

B. Small-scale fading

The coefficient of variation particularized with the statistical conditional model can easily be proven to be:

$$CV^2_{\|\mathbf{c}\|^2} = \mathcal{E}^2(\mathcal{A}_{tx},\mathcal{D}_{tx})\mathcal{E}^2(\mathcal{A}_{rx},\mathcal{D}_{rx})\alpha^2(\mathbf{c})$$
$$\text{where } \alpha^2(\mathbf{c}) = 1 - \frac{\mathbb{E}_{\mathbf{c}|\|\mathbf{c}\|^2}\left\{\|\mathbf{c}\|_4^4\right\}}{\|\mathbf{c}\|^4}. \quad (8)$$

The small-scale fading contribution to CV^2 thus consists of a product of the quantities defined in (6) that depend only on the antenna array topologies ($\mathcal{A}_{tx}$/$\mathcal{A}_{rx}$) and ray distributions ($\mathcal{D}_{tx}$/$\mathcal{D}_{rx}$) multiplied by a propagation conditions factor $\alpha^2(\mathbf{c})$ that depends only on the statistics of the ray powers $\mathbf{c}$.

Ray correlations: Array topologies. This paragraph focuses on the influence of $\mathcal{A}_{tx}$ on the quantity $\mathcal{E}^2(\mathcal{A}_{tx},\ \mathcal{D}_{tx})$ (the study is done only at the emitter, the obtained results being equally valid at the receiver). A uniform distribution of the rays over the unit sphere is considered ($\mathcal{D}_{tx} = \mathcal{U}_{\mathcal{S}_2}$). Eq. (6) yields

$$\mathcal{E}^2(\mathcal{A}_{tx},\ \mathcal{D}_{tx}) = \frac{1}{N_t^2}\mathbb{E}\left\{\left|\sum_{i=1}^{N_t} \mathrm{e}^{2j\pi\frac{\vec{a}_{tx,i}\cdot(\vec{u}_{tx,p}-\vec{u}_{tx,p'})}{\lambda}}\right|^2\right\}.$$

A well-known situation is when the inner sum involves exponentials of independent uniformly distributed phases and hence corresponds to a random walk with N_t steps of unit length. The above expectation then consists in the second moment of a Rayleigh distribution and $\mathcal{E}^2(\mathcal{A}_{tx},\ \mathcal{D}_{tx}) = \frac{1}{N_t}$. A necessary condition to such a case is to have (at least) a half wavelength antenna spacing Δd to ensure that phases are spread over $[0,\ 2\pi]$. On the other hand, phase independences are expected to occur for asymptotically large Δd. It is however shown hereafter that such assumption turns out to be valid for much more reasonable value of Δd.

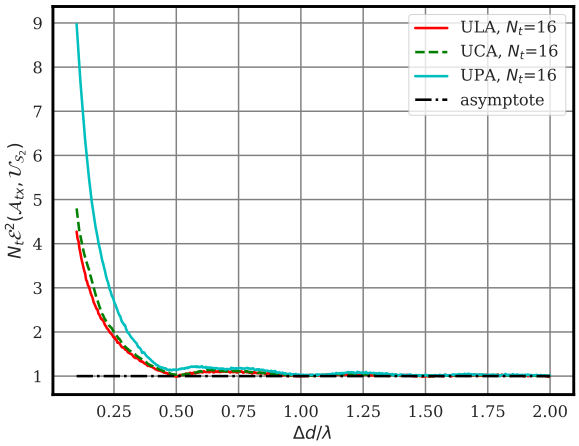


Fig. 2. Numerical evaluation of $\mathcal{E}(\mathcal{A}_{tx},\mathcal{U}_{\mathcal{S}_2})$ for various array types and increasing antenna spacing Δd. The values are normalized so the asymptote is 1.

Numerical evaluations of $\mathcal{E}^2$ are performed versus Δd (Fig. 2), and versus N_t (Fig. 3). Uniformly distributed rays over the 3D unit sphere ($\mathcal{D}_{tx} = \mathcal{D}_{rx} = \mathcal{U}_{\mathcal{S}_2}$) and Uniform Linear, Circular and Planar Arrays (ULA, UCA and UPA) are considered. As a reminder, the smaller $\mathcal{E}(\mathcal{A}_{tx},\mathcal{D}_{tx})$ the better the channel hardening. In Fig. 2, $\mathcal{E}^2$ reaches the asymptote $1/N_t$ for all array types with $\Delta d = \frac{\lambda}{2}$ and remains almost constant for larger Δd. Fig. 3 shows that $\mathcal{E}^2$ merely follows the $1/N_t$ law whatever the array type. We thus conclude that the independent uniform phases situation discussed above is a sufficient model for any array topology given that $\Delta d \geq \frac{\lambda}{2}$. It is therefore assumed in the sequel that,

$$\mathcal{E}^2(\mathcal{A}_{tx},\mathcal{U}_{\mathcal{S}_2}) \approx 1/N_t, \quad \mathcal{E}^2(\mathcal{A}_{rx},\mathcal{U}_{\mathcal{S}_2}) \approx 1/N_r.$$

Ray correlation: Ray distributions. In a mobility scenario, random translations and rotations might affect the receiver, leading to the previously used uniform distribution of the received rays over the unit sphere. However emitted rays at the base station may have much more constrained distributions

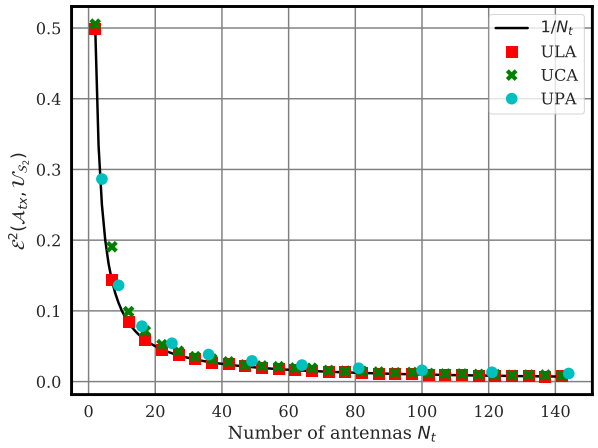


Fig. 3. Numerical evaluation of $\mathcal{E}(\mathcal{A}_{tx}, \mathcal{U}_{\mathcal{S}_2})$ for various antenna arrays at the half wavelength. The lower, the better.

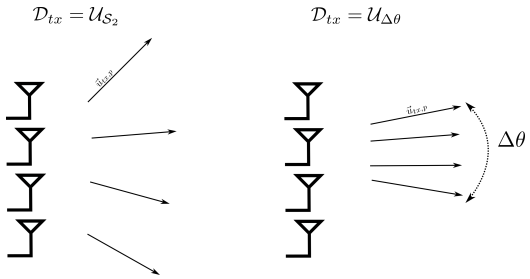


Fig. 4. On the leftmost side, uniform distribution of the rays on the unit sphere $\mathcal{U}_{\mathcal{S}_2}$. On the rightmost side, constrained distribution of the rays with solid angle $\mathcal{U}_{\Delta\theta}$

(especially in the elevation plane). The formula 7 is also valid for those cases but the $\mathcal{E}(\mathcal{A}_{tx}, \mathcal{D}_{tx})$ term shall be re-evaluated.

We study the ULA case with uniform AoD distribution with constrained elevation in the interval $[-\Delta\theta/2, \Delta\theta/2]$ illustrated on Fig. 4. This distribution is denoted $\mathcal{U}_{\Delta\theta}$. We have the equality $\mathcal{U}_{\pi} = \mathcal{U}_{\mathcal{S}_2}$.

The behavior of $\mathcal{E}(\mathcal{A}_{tx}, \mathcal{U}_{\Delta\theta})$ for increasing number of antennas is given by Fig 5. We can observe a clear degradation when $\Delta\theta$ decreases. This is coherent with literature on channel hardening, constrained rays induce correlated channel matrices, mitigating the channel hardening effect. This model asymptotically leads to the pinhole channel that is known to not harden [4]. Fig. 6 shows the effect of antenna spacing on $\mathcal{E}(\mathcal{A}_{tx}, \mathcal{U}_{\Delta\theta})$. It can be observed on this figure that the channel hardening loss due to restricted distribution of the rays by $\Delta\theta$ can be compensated by increasing antenna spacing above the half-wavelength. The influence of $\Delta\theta$ on channel hardening is depicted by Fig. 7. A clear reduction of channel hardening can be observed when θ decreases.

Propagation conditions. It is now interesting to point out that the propagation factor $\alpha(\mathbf{c})$ introduced in (8) is bounded by

$$0 \leq \alpha^2(\mathbf{c}) \leq 1 - 1/P. \tag{9}$$

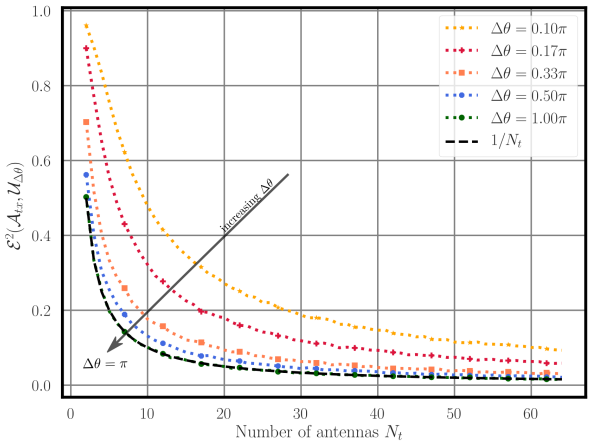


Fig. 5. Numerical evaluation of $\mathcal{E}(\mathcal{A}_{tx}, \mathcal{U}_{\Delta\theta})$ for increasing $\Delta\theta$ with fixed half-wavelength antenna spacing. The lower, the better.

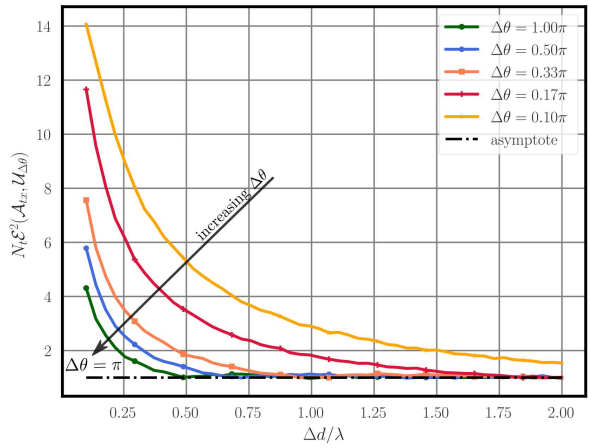


Fig. 6. Numerical evaluation of $\mathcal{E}(\mathcal{A}_{tx}, \mathcal{U}_{\Delta\theta})$ for increasing $\Delta\theta$ with fixed number of antennas $N_t = 16$. The lower, the better.

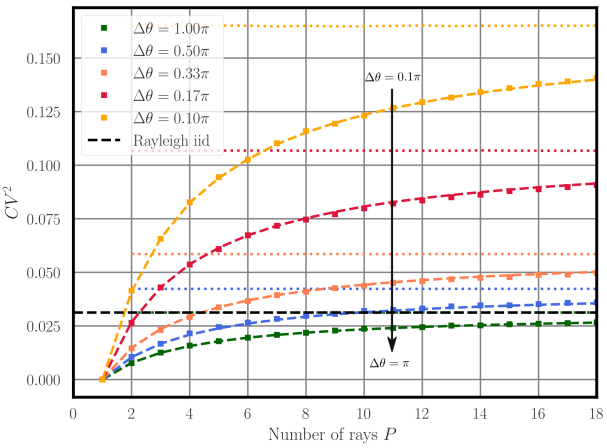


Fig. 7. Comparison between (7), simulated CV^2 and correlated Rayleigh, the dashed, squared and dotted lines respectively. A 16×2 ULA setup is considered. Uniform distribution of DoDs and DoAs with constrained DoDs and complex Gaussian gains. The large-scale factor is normalized.

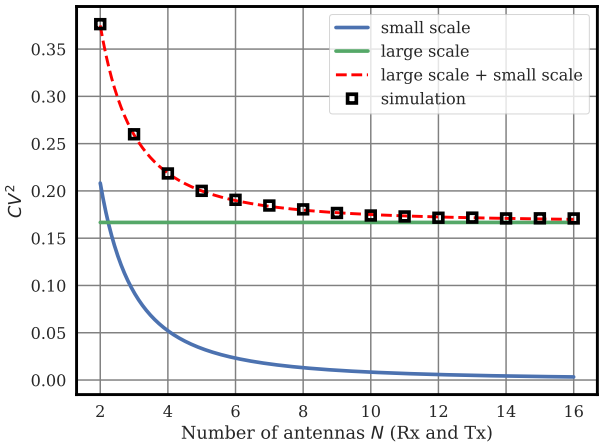


Fig. 8. Comparison between (7) and simulated CV^2. Uniform distribution of DoDs and DoAs over the unit sphere and complex Gaussian gains.

Those bounds are deduced from the following inequality:

$$\|\mathbf{c}\|_2^4/P \leq \|\mathbf{c}\|_4^4 \leq \|\mathbf{c}\|_2^4. \tag{10}$$

The right inequality comes from the convexity of the square function. Equality is achieved when there is only one contributing ray, i.e. no multipath occurs. In that case $CV^2_{\|\mathbf{c}\|^2} = 0$ and the MIMO channel power is deterministic. The left part in (10) is given by Hölder's inequality. Equality is achieved when there are P rays of equal power. Then, taking the expectation on each member in (10) yields (9).

In contrast to the large-scale fading, more rays lead to more small-scale fluctuations. It is indeed well known that a richer scattering environment increases small-scale fading.

Comparison with the simulations. Based on the general formula given in (7), on the interpretations and evaluations of its terms, we can derive the expression of channel hardening for the illustrating simulations of Section III-D:

$$CV^2_{\text{illustration}} = \frac{1}{N_t N_r}(1 - 1/P) + 1/P.$$

Simulation and approximated formula are compared in Fig. 8 in which small-scale and large-scale contributions are easily evidenced, as intuitively expected from simulations of Fig. 1.

C. Comparison with Rayleigh channel models

In this section we compare our channel hardening expression conditioned by $\|\mathbf{c}\|^2$ (local behavior) to the correlated Rayleigh fading channel in both strong scattering and low scattering situations.

In the high scattering regime, the correlated Rayleigh channels approach is known to perform well. Without any particular constraint on the DoD and DoA, the correlation matrix is given by $\mathbf{R} = \mathbf{Id}$ (the well-known Rayleigh i.i.d. channel model). Using this result with (4) yields

$$CV^2_{iid} = \frac{1}{N_t N_r}.$$

Using the realistic model in a rich scattering environment, the propagation term $\alpha(\mathbf{c})$ of small-scale variations (8) reaches the upper bound of (9). This yields the limit

$$CV^2 \xrightarrow{P\to\infty} CV^2_{iid} \tag{11}$$

which is coherent with the interpretation of the model. This behavior can be observed on the lowest curve of Fig. 7.

However in the low scattering regime (considering P rays), the Rayleigh modeling approach is not valid any more. The sparse channel is not modeled properly and formula (4) underestimates the channel hardening effect. Our approach introduces a propagation factor $\alpha(\mathbf{c})$ that models the scattering effect and the sparsity of the channel. According to results given by the ray-based model Fig. (7), channel hardening is increased in low scattering scenarios and reaches the correlated Rayleigh hardening for $P \to \infty$, which is consistent with the previous physical interpretation.

VI. Conclusion

In this paper, previous studies on channel hardening have been extended using a physics-based model. We have separated influences of antenna array topologies and propagation characteristics on the channel hardening phenomenon. Large-scale and small-scale contributions to channel variations have been evidenced. Essentially, this paper provides a general framework to study channel hardening using accurate propagation models.

To illustrate the overall behavior of channel hardening, this framework have been used with generic model parameters and hypotheses. The scaling laws evidenced for simpler channel models are conserved provided the antennas are spaced by at least half a wavelength. The results are consistent with state of the art and provide further insights on the influence of array topology and propagation on channel hardening. The proposed expression can easily be exploited with various propagation environments and array topologies to provide a more precise understanding of the phenomenon compared to classical channel descriptions based on Rayleigh fading models.

Acknowledgment

This work has been performed in the framework of the Horizon 2020 project ONE5G (ICT-760809) receiving funds from the European Union. The authors would like to acknowledge the contributions of their colleagues in the project, although the views expressed in this contribution are those of the authors and do not necessarily represent the project.

Appendix A
Coefficient of variation (7)

For the sake of simplicity, an intermediary matrix $\mathbf{A}$ is introduced. It is defined by

$$[\mathbf{A}]_{p,p'} = \begin{cases} 2|\gamma_{p,p'}|\cos(\phi_{p,p'}) & \text{if } p \neq p' \\ 1 & \text{if } p = p' \end{cases}$$

with $\phi_{p,p'} = \arg(c_p^* c_{p'} \gamma_{p,p'})$ the whole channel phase dependence. $\|\mathbf{H}\|_F^2$ can be written using a quadratic form with vector

$\mathbf{c}$ and matrix $\mathbf{A}$, which can be decomposed into two terms $\mathbf{I}$ (identity) and $\mathbf{J}$

$$\frac{\|\mathbf{H}\|_F^2}{N_t N_r} = \mathbf{c}^T \mathbf{A} \mathbf{c} = \mathbf{c}^T \mathbf{c} + \mathbf{c}^T \mathbf{J} \mathbf{c}$$

where $\mathbf{J} = \mathbf{A} - \mathbf{I}$. $\mathbb{E}\{\mathbf{J}\} = \mathbf{0}$ so:

$$\frac{\mathbb{E}\left\{\|\mathbf{H}\|_F^4\right\}}{(N_t N_r)^2} = \mathbb{E}\left\{\|\mathbf{c}\|^4\right\} + \mathbb{E}\left\{(\mathbf{c}^T \mathbf{J} \mathbf{c})^2\right\}.$$

The ray independence properties yields the following weighted sum of coupled ray powers

$$\mathbb{E}\left\{(\mathbf{c}^T \mathbf{J} \mathbf{c})^2\right\} = \sum_{p \neq p'} \mathbb{E}\left\{|c_p|^2 |c_{p'}|^2\right\} \mathbb{E}\left\{[\mathbf{J}]_{p,p'}^2\right\}.$$

Considering i.i.d. rays, all the weights $\mathbb{E}\left\{[\mathbf{J}]_{p,p'}^2\right\}$ are identical. Using the weights notations introduced in (6) and the definition of the 4-norm yields the second order moment $\mathbb{E}\left\{\|\mathbf{H}\|_F^4\right\}$. With the expectation (5) we derive the result (7).

REFERENCES

[1] E. Telatar, "Capacity of Multi-antenna Gaussian Channels," *European Transactions on Telecommunications*, vol. 10, no. 6, pp. 585–595, Nov. 1999.

[2] T. L. Marzetta, *Fundamentals of massive MIMO*. Cambridge University Press, 2016.

[3] B. M. Hochwald, T. L. Marzetta, and V. Tarokh, "Multiple-antenna channel hardening and its implications for rate feedback and scheduling," *IEEE transactions on Information Theory*, vol. 50, no. 9, pp. 1893–1909, 2004.

[4] H. Q. Ngo and E. G. Larsson, "No downlink pilots are needed in TDD massive MIMO," *IEEE Transactions on Wireless Communications*, vol. 16, no. 5, pp. 2921–2935, 2017.

[5] E. Björnson, E. de Carvalho, E. G. Larsson, and P. Popovski, "Random access protocol for massive MIMO: Strongest-user collision resolution (SUCR)," in *2016 IEEE International Conference on Communications (ICC)*, May 2016, pp. 1–6.

[6] l. O. Martínez, E. De Carvalho, and J. O. Nielsen, "Massive MIMO properties based on measured channels: Channel hardening, user decorrelation and channel sparsity," in *Signals, Systems and Computers, 2016 50th Asilomar Conference on*. IEEE, 2016, pp. 1804–1808.

[7] S. Gunnarsson, J. Flordelis, L. V. der Perre, and F. Tufvesson, "Channel hardening in massive MIMO - A measurement based analysis," *CoRR*, vol. abs/1804.01690, 2018. [Online]. Available: http://arxiv.org/abs/1804.01690

[8] E. Björnson, J. Hoydis, and L. Sanguinetti, "Massive MIMO Networks: Spectral, Energy, and Hardware Efficiency," *Foundations and Trends in Signal Processing*, vol. 11, no. 3-4, pp. 154–655, 2017.

[9] S. Loyka and G. Levin, "On physically-based normalization of MIMO channel matrices," *IEEE Transactions on Wireless Communications*, vol. 8, no. 3, pp. 1107–1112, 2009.

[10] V. Raghavan and A. M. Sayeed, "Sublinear Capacity Scaling Laws for Sparse MIMO Channels," *IEEE Transactions on Information Theory*, vol. 57, no. 1, pp. 345–364, Jan. 2011.

[11] T. Zwick, C. Fischer, and W. Wiesbeck, "A stochastic multipath channel model including path directions for indoor environments," *IEEE Journal on Selected Areas in Communications*, vol. 20, no. 6, pp. 1178–1192, Aug. 2002.

[12] M. K. Samimi, G. R. MacCartney, S. Sun, and T. S. Rappaport, "28 GHz Millimeter-Wave Ultrawideband Small-Scale Fading Models in Wireless Channels," in *2016 IEEE 83rd Vehicular Technology Conference (VTC Spring)*, May 2016, pp. 1–6.

[13] L. Le Magoarou and S. Paquelet, "Parametric channel estimation for massive MIMO," *arXiv preprint arXiv:1710.08214*, 2017.

[14] S. Sun, G. R. MacCartney Jr., and T. S. Rappaport, "A novel millimeter-wave channel simulator and applications for 5G wireless communications," *CoRR*, vol. abs/1703.08232, 2017. [Online]. Available: http://arxiv.org/abs/1703.08232

[15] A. A. Saleh and R. Valenzuela, "A statistical model for indoor multipath propagation," *IEEE Journal on selected areas in communications*, vol. 5, no. 2, pp. 128–137, 1987.

[16] X. Wu, C.-X. Wang, J. Sun, J. Huang, R. Feng, Y. Yang, and X. Ge, "60-GHz Millimeter-Wave Channel Measurements and Modeling for Indoor Office Environments," *IEEE Transactions on Antennas and Propagation*, vol. 65, no. 4, pp. 1912–1924, Apr. 2017.